PAPER

Check for updates

Structure and luminescence properties of a novel broadband green-emitting oxyapatite-type phosphor

Na An,[ab] Fei Xu,[c] Qingfeng Guo, [ID] *[ab] Libing Liao, [ID] *[d] Lefu Mei[d] and Haikun Liu[d]

In recent years, synthetic apatite-doped rare-earth luminescent materials and their optical properties have attracted extensive worldwide attention. In this study, a series of novel green phosphors $Sr_2Y_3(SiO_4)_2(PO_4)$O:Eu^{2+} with apatite structure was fabricated *via* a high temperature solid-state reaction. X-ray diffraction, structure refinement, photoluminescence excitation, emission spectra, and temperature-dependent emission intensity were employed to describe the phase and property of the samples. Under the excitation of 365 nm, the phosphors emit strong green emission in the broad band range from 400 nm to 700 nm, which almost covers the visible light spectrum. The quenching concentration of Eu^{2+} in $Sr_2Y_3(SiO_4)_2(PO_4)$O was about 0.05, which was attributed to the dipole–dipole interactions. The evidence that the as-prepared phosphor can be successfully excited by near ultraviolet light indicates that it can be potentially used as a near UV-convertible phosphor for white light-emitting diodes.

1. Introduction

It is well known that energy efficiency is one of the key parameters in illumination sources and other pervasive products. White light-emitting diodes (wLEDs) have bright future in traffic lights, displays, general lighting, and decorative lighting owing to their high efficiency and environment friendly nature.[1–3] Currently, phosphor-converted wLEDs combining tricolor phosphors and near ultraviolet (n-UV) or blue chips have been extensively applied as solid-state lighting sources owing to their excellent performance and properties, *e.g.*, long life, conversion efficiency, high color-rending index, and lower power consumption.[4–6]

In general, a phosphor is composed of hosts and activators (sometimes sensitizers are also included).[7] Rare-earth (RE) ions (Ce^{3+}, Eu^{2+}, and Tb^{3+}) can be used as activators for white light-emitting diodes (wLEDs). The emission color changes when the RE ions are doped into different hosts derived from their 4f–4f or 4f–5d transitions.[8,9] Eu^{2+} with a wide emission color range is a popular activator with intensive absorption in the UV and visible regions.[10–14] Transitions between the ground state (4f energy level) and the excited 5d-state of Eu^{2+} can be influenced

by the crystal lattice pattern, *e.g.*, crystal-field strength, atom coordination, and covalence.[15–17] Moreover, the careful selection of the host material is also critical since the host structure will affect the crystal field environment of the RE ions, which will change the energy transitions of the RE ions.[18] A deeper understanding of the crystal structure of the targeted compound is necessary for choosing the host material because there are at least two or three suitable non-equivalent crystallographic sites for the Eu^{2+} occupation that can regulate the crystal field environment of Eu^{2+}.[19] Accordingly, efforts have been devoted for the development of novel host materials, containing abundant cationic crystallographic sites doped with Eu^{2+}, which can be typically excited by n-UV light.[20–23]

The apatite-type structured compounds have two nonequivalent cationic sites for the Eu^{2+} occupation, which enables them to be one of the most potential phosphor host materials.[24,25] In general, compounds with the apatite structure are characterized by a general chemical formula of $M_{10}[XO_4]_6Y_2$, where M is defined as a divalent cation (Mg^{2+}, Ca^{2+}, Ba^{2+}, *etc.*), whereas rare-earth ions (Y^{3+}, La^{3+}, Eu^{2+} *etc.*), alkali metal ions (Na$^+$, K$^+$, Ag$^+$, *etc.*) can also enter the M-site, thus forming a coupling isomorphic substitution. $[XO_4]$ is defined as a complex anionic group ([PO$_4$], [VO$_4$], [AsO$_4$], *etc.*), and Y commonly represents the anions such as F$^-$, Br$^-$, or OH$^-$.[26] In the past few decades, Eu^{2+}-doped apatite phosphors have attracted considerable attention worldwide, *e.g.*, $Ca_5(PO_4)_3F$,[27] $Sr_5(PO_4)_3Cl$,[28] $Ca_8Gd_2(PO_4)_6O_2$,[29] and $Ca_2Ba_3(PO_4)_3Cl$.[30] However, no report is available on the Eu^{2+}-doped $Sr_2Y_3(SiO_4)_2(PO_4)O_2$ phosphor with the apatite structure. On the other hand, developing novel apatite phosphors doped with Eu^{2+} that can be excited by n-UV light (350–420 nm) has a significant practical value.

^{a}School of Gemology, China University of Geosciences, Beijing 100083, China. E-mail: qfguo@cugb.edu.cn

^{b}Jewelry and Mineral Materials Laboratory of Experimental Teaching Demonstration Center, Beijing, China

^{c}Academy of Arts & Design, Tsinghua University, Beijing 100084, China

^{d}Beijing Key Laboratory of Materials Utilization of Nonmetallic Minerals and Solid Wastes, National Laboratory of Mineral Materials, School of Materials Sciences and Technology, China University of Geosciences, Beijing 100083, China. E-mail: clayl@cugb.edu.cn

Herein, a novel apatite-type phosphor $Sr_2Y_3(SiO_4)_2(PO_4)$ $O:Eu^{2+}$, emitting green fluorescence, was successfully prepared *via* a high-temperature solid-state reaction,. The crystal structure of the as-prepared sample was identified by the Rietveld refinement method in detail, which was used to study how the crystal structure and composition affected the luminescence property of the sample. In addition, the thermal luminescence property of the phosphor has also been revealed in this study. Under 365 nm excitation, the phosphor exhibits a strong green emission at 505 nm with an obvious band ranging from 400 nm to 700 nm, which almost covers the visible light spectrum. The results indicate that the $Sr_2Y_3(SiO_4)_2(PO_4)O:Eu^{2+}$ phosphor can act as a potential green phosphor for n-UV phosphor-converted wLEDs.

2. Experimental procedure

2.1. Materials and synthesis

The $Sr_2Y_3(SiO_4)_2(PO_4)O:Eu^{2+}$ phosphor was synthesized using the traditional high-temperature solid-phase synthesis method with starting materials, including $SrCO_3$ (Aldrich, 99.9%), Y_2O_3 (Aldrich, 99.99%), $NH_4H_2PO_4$ (Aldrich, 99.9%), SiO_2 (Aldrich, 99.99%), and Eu_2O_3 (Aldrich, 99.999%). First, they were weighed in an electronic balance according to the stoichiometric ratio. Then, they were mixed and ground thoroughly in an agate mortar. Further, the raw materials were preheated at 500 °C for 3 h in a furnace and moved into alumina crucibles after being cooled down to room temperature. In addition, the preliminary products were annealed at 1400 °C for 5 h under a reducing atmosphere (10% H_2 + 90% N_2). When the furnace was cooled down to room temperature again, the final product was smashed and re-ground for subsequent tests.

2.2. Characterization

The phase structure of each sample was evaluated using an X-ray powder diffractometer (RigakuDmax 12 kW, Japan) with Cu Kα radiation ($\lambda = 0.15418$ nm) from 10° to 70° (2θ). The Rietveld refinement of $Sr_{3.95}Y_6(SiO_4)_4(PO_4)_2O_2:0.05Eu^{2+}$ was carried out by the TOPAS software. Photoluminescence and excitation spectra of the sample were recorded using a fluorescence spectrofluorometer (FL-4600, HITACHI, Japan) fitted with a 700 V and 150 W Xe lamp source. Lifetime of the samples was tested using a spectrometer (HORIBA JOBIN YVON FL3-21) with excitation by a pulsed radiation laser at 370 nm.

3. Results and discussions

Fig. 1 presents the XRD patterns of $Sr_{(2-x)}Y_3(SiO_4)_2(PO_4)O:xEu^{2+}$ ($x = 0.01$ and 0.05) and the referred standard data for $Ca_8Nd_2(PO_4)_6O_2$ (PDF-32-175). The diffraction peaks of the $Sr_{(2-x)}Y_3(SiO_4)_2(PO_4)O:xEu^{2+}$ phosphors are consistent with those of the $Ca_8Nd_2(PO_4)_6O_2$ (Fig. 1), where a minor deviation of the dominant diffraction peak at higher 2θ can be found due to the replacement of Sr by Eu, indicating that a small amount of Eu^{2+} doping does not lead to a variation in the structure.

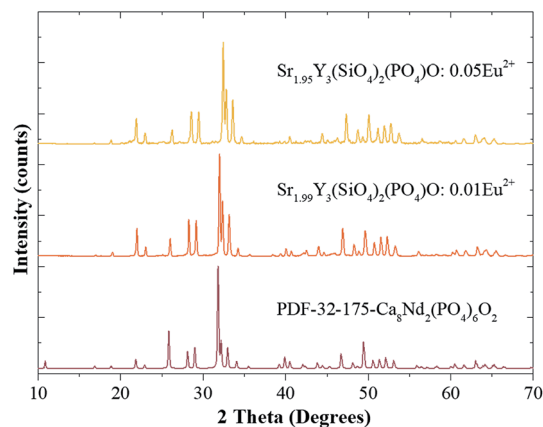**Fig. 1** The XRD patterns of $Sr_{(2-x)}Y_3(SiO_4)_2(PO_4)O:xEu^{2+}$ ($x = 0.01$ and 0.05), and the standard card (PDF-32-175-$Ca_8Nd_2(PO_4)_6O_2$) is shown as a reference.

To further investigate the phase purity and occupation of Eu^{2+}, TOPAS 4.2 (ref. 31) was used to analyze the Rietveld refinement. The structure of $Ca_8Nd_2(PO_4)_6O_2$, possessing a hexagonal structure with the space group $P6_3/m$, was employed as the initial model.[32] Silicon oxygen tetrahedron and phosphorus oxygen tetrahedron is independent with each other Sr1 and Sr2 occupy two independent sites for Sr^{2+} in the crystal lattice. Sr1 is in a 9-fold coordination state, and Sr2 is in a 7-fold coordination state. Similar to Sr^{2+}, the radii of Eu^{2+} in the 7-fold coordination and 9-fold coordination sites are 0.120 and 0.130 nm, respectively. Eu^{2+} can occupy the two positions of Sr^{2+}. The Rietveld analysis patterns for the X-ray power diffraction data of $Sr_{3.95}Y_6(SiO_4)_4(PO_4)_2O_2:0.05Eu^{2+}$ is shown in Fig. 2. The occupation of the cations was set to a fixed value according the chemical formula. The fractional atomic coordinates, isotropic displacement parameters, and the cell parameters were refined. The atomic coordinates, occupancies and
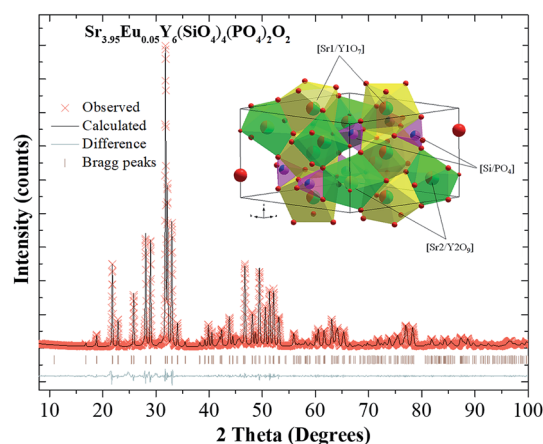

Fig. 2 XRD refinement result of the $Sr_{3.95}Eu_{0.05}Y_6(SiO_4)_4(PO_4)_2O_2$ sample: experimental results (×), calculated results (|), and their difference (bottom). The brown solid lines represent the Bragg reflection positions, and the inset shows a crystal structure diagram of the host.

Table 1 Crystal structural data and lattice parameters for $Sr_{3.95}Y_6(SiO_4)_4(PO_4)_2O_2$:0.05Eu^{2+}

Formula	$Sr_{3.95}Y_6(SiO_4)_4(PO_4)_2O_2$:0.05Eu^{2+}
Space group	$P6_3/m$ – hexagonal
Cell parameters	$a = b = 9.477(10)$ Å, $c = 6.954(80)$ Å
	$\alpha = 90°$, $\beta = 90°$, $\gamma = 120°$
	$V = 540.53(16)$ Å, $Z = 2$
Reliability factors	$R_{wp} = 8.89\%$
	$R_p = 6.66\%$
	$\chi^2 = 3.64$

displacement parameters (Å^2) are listed in Table 1, and the cell parameters and reliability factors are listed in Table 2. The cell parameters are $a = b = 9.477(10)$ Å, $c = 6.954(80)$ Å, $\alpha = 90°$, $\beta = 90°$, $\gamma = 120°$, and $V = 540.53(16)$ Å. The refinement was stable and the fit is convincing with low R-factors, which verify the phase purity of the as-prepared sample.

The photoluminescence excitation and emission spectra of the $Sr_{3.95}Y_6(SiO_4)_4(PO_4)_2O_2$:0.05Eu^{2+} are given in Fig. 3(a). It is clear that the PLE spectrum has an absorption band at 274 nm, which resulted from the 4f–5d transitions in Eu^{2+}. The PL spectrum exhibits a green emission peak at 505 nm, which can be decomposed into two sub-bands with Gauss imitating decomposition at 498 nm and 555 nm, respectively (Fig. 3(b)). Therefore, Eu^{2+} can occupy two cationic lattices, which is

consistent with the refined results. The lattice site centers of Eu^{2+} can be determined using the van Uitert empirical equation:[33]

$$E = Q\left[1 - \left(\frac{V}{4}\right)^{\frac{1}{V}} 10^{-\frac{n \times E_a \times r}{80}}\right] \quad (1)$$

where E is the position of the low-energy of the 5f excited-state (cm^{-1}) or the emission peak of Eu^{2+}, Q is 34 000 cm^{-1}, V is 2, n is the anion number around Eu^{2+}, E_a is a constant, r is the effective radius of Sr^{2+} (nm). Therefore, E is negatively correlated with n. Two different luminescent centers, having nine and seven coordinations, contribute to the fluorescence emission peaks at 498 and 555 nm, respectively.

Fig. 4(a) shows PL spectra of $Sr_{(4-x)}Y_6(SiO_4)_4(PO_4)_2O_2$:$x$Eu^{2+} ($x = 0.01, 0.03, 0.05, 0.07, 0.09,$ and 0.12). It can be seen that the luminescence intensity increases first and then decreases. The luminescence properties of phosphors mainly depend on the rare-earth ion content, $e.g.$, the luminous intensity is the highest when Eu^{2+} is 0.05.

As shown in Fig. 4(b), the luminescence intensity of Eu^{2+} first increases with the increase in the Eu^{2+} concentration, and reaches the maximum when $x = 0.05$; further, the emission intensity decreases caused by the concentration quenching effect. The concentration quenching is caused by the energy transfer of Eu^{2+}. In order to establish the concentration

Table 2 Fractional atomic coordinates and isotropic displacement parameters (Å^2) of $Sr_{3.95}Y_6(SiO_4)_4(PO_4)_2O_2$:0.05Eu^{2+}

Atom	x	y	z	Occupancy	$U_{iso}/$Å^2
Sr1(Eu1)/Y1	1/3	2/3	0	0.35(0.05)/0.6	0.0292(7)
Sr2(Eu2)/Y2	0.24632(0)	0.23413(5)	1/4	0.35(0.05)/0.6	0.0250(2)
P1/Si1	0.03324(1)	0.40456(0)	1/4	0.33/0.67	0.0239(3)
O1	0.48621(8)	0.15352(7)	1/4	1	0.0431(0)
O2	0.12523(5)	0.59325(1)	1/4	1	0.0341(2)
O3	0.11200(4)	0.34721(7)	0.07382(0)	1	0.0181(6)
O4	0	0	1/4	1	0.0197(3)
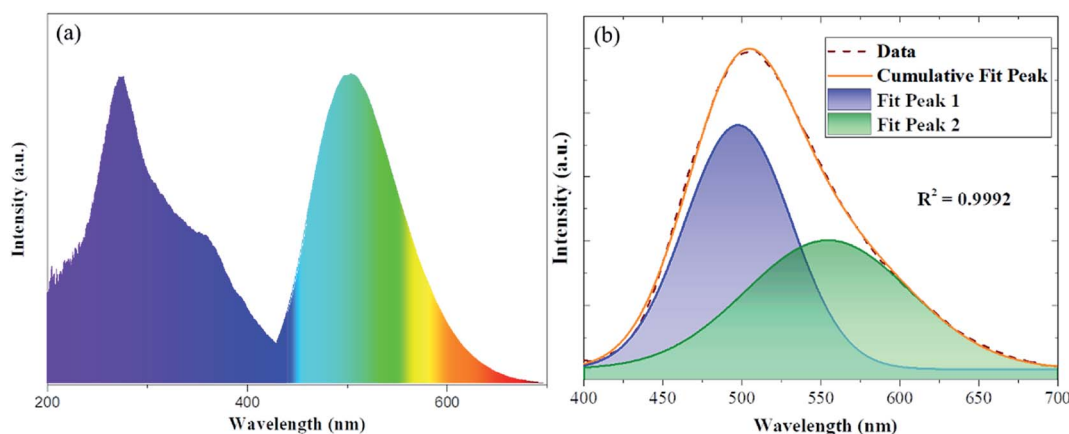
Fig. 3 (a) Excitation and emission spectra of the $Sr_{3.95}Y_6(SiO_4)_4(PO_4)_2O_2$:0.05Eu^{2+} sample, (b) PL spectrum of $Sr_{3.95}Y_6(SiO_4)_4(PO_4)_2O_2$:0.05Eu^{2+} excited at 365 nm and Gaussian fitting result. Two Gaussian components are peaked at 498 nm and 555 nm.

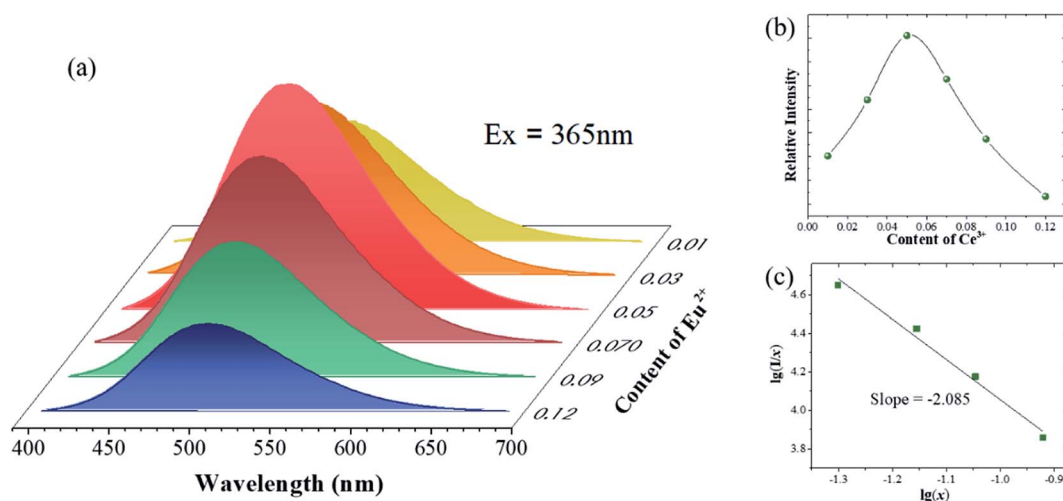Fig. 4 (a) PL spectra of $Sr_{(4-x)}Y_6(SiO_4)_4(PO_4)_2O_2$:$xEu^{2+}$ (x = 0.01, 0.03, 0.05, 0.07, 0.09, and 0.12) under the excitation of 365 nm, (b) intensities of Eu^{2+} as a function of Eu^{2+} doping concentration, and (c) linear fitting of log(x) *versus* log(I/x) in the $Sr_{3.95}Y_6(SiO_4)_4(PO_4)_2O_2$:$0.05Eu^{2+}$ samples.

quenching mechanism, the critical energy transfer distance R_C can be calculated first:[34]

$$R_C \approx 2\left[\frac{3V}{4\pi x_C N}\right]^{\frac{1}{3}} \qquad (2)$$

For the host with x_C = 0.05, V = 540.53 Å^3, N = 10, the obtained critical distance R_C is 12.74 Å. According to Dexter theory, when the R_C value is >5, a non-radiative transition occurs between the Eu^{2+} ions; therefore, the type of energy transfer can be described as follows:[35,36]

$$\frac{I}{x} = K\left[1 + \beta(x)^{\frac{\theta}{3}}\right]^{-1} \qquad (3)$$

where I is the emission intensity and x is the activator concentration of Eu^{2+}, θ = 6, 8, and 10 for dipole–dipole (d–d), dipole–quadrupole (d–q), and quadrupole–quadrupole (q–q), respectively.[37,38] Fig. 4(c) shows the relational curve between log(I/x) and log(x) in the $Sr_{3.95}Y_6(SiO_4)_4(PO_4)_2O_2$:$0.05Eu^{2+}$ phosphors under the 365 nm light irradiation with line slope of −2.085, and the calculated θ value based on eqn (3) is 6.255, which means that the concentration quenching mechanism of Eu^{2+} in the sample is d–d.

The PL decay curve of the Eu^{2+} phosphor was detected at 365 nm, which can be used to determine the fluorescence lifetime. Fig. 5 describes the decay curves of the phosphor, which can be fitted by a double-exponential equation:[39,40]

$$I = A_1 \times \exp\left(\frac{-t}{\tau_1}\right) + A_2 \exp\left(\frac{-t}{\tau_2}\right) + I_0 \qquad (4)$$

where I_0 is the initial emission intensity, t represents time, A_1 and A_2 are invariant constants after fitting, and τ_1 and τ_2 are two different decay lives. The calculated Eu^{2+} lifetime is 0.613 μs.

The variable temperature fluorescence test was carried out to show the thermal stability of the sample. Fig. 6(a) presents the relationship between the emitted light color and the ambient

temperature in the wavelength range from 400 to 700 nm. As shown in Fig. 6(b), the emission intensity of the sample is 63% of that at room temperature with the temperature rising to 150 °C, indicating an excellent thermal stability. In addition, the strongest emission peak moves from 502 to 490 nm. The emission band has slight blue shift with an increase in temperature. The activation energy (E) can be obtained by the Arrhenius equation:[41,42]

$$\ln\left(\frac{I_0}{I}\right) = \ln A - \left(\frac{E}{kT}\right) \qquad (5)$$

where $I(0)$ is the initial emission intensity of the phosphor at 25 °C and $I(T)$ is the emission intensity at different temperatures, c is constant, E is the activation energy for thermal quenching, and k is the Boltzmann constant (8.617×10^{-5} eV). The plot of $\ln[(I_0/I)^{-1}]$ *vs.* $1/kT$ in Fig. 6(c) follows a line trend, obtaining 0.210 eV as the activation energy E. Fig. 6(d) shows that the calculated CIE chromaticity coordinates of $Sr_{3.95}Y_6(SiO_4)_4(PO_4)_2O_2$:$0.05Eu^{2+}$ is (0.233, 0.446), and the green
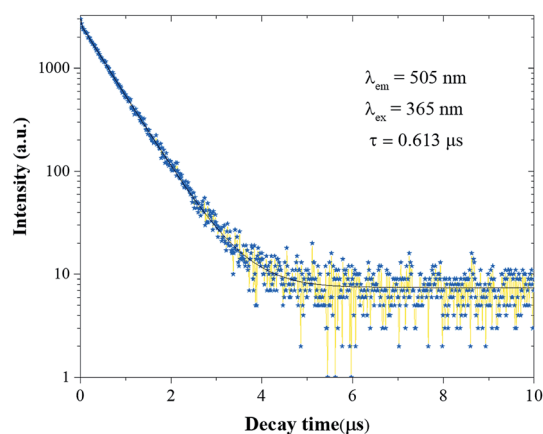
Fig. 5 Decay curves of Eu^{2+} in the $Sr_{3.95}Y_6(SiO_4)_4(PO_4)_2O_2$:$0.05Eu^{2+}$ phosphor.
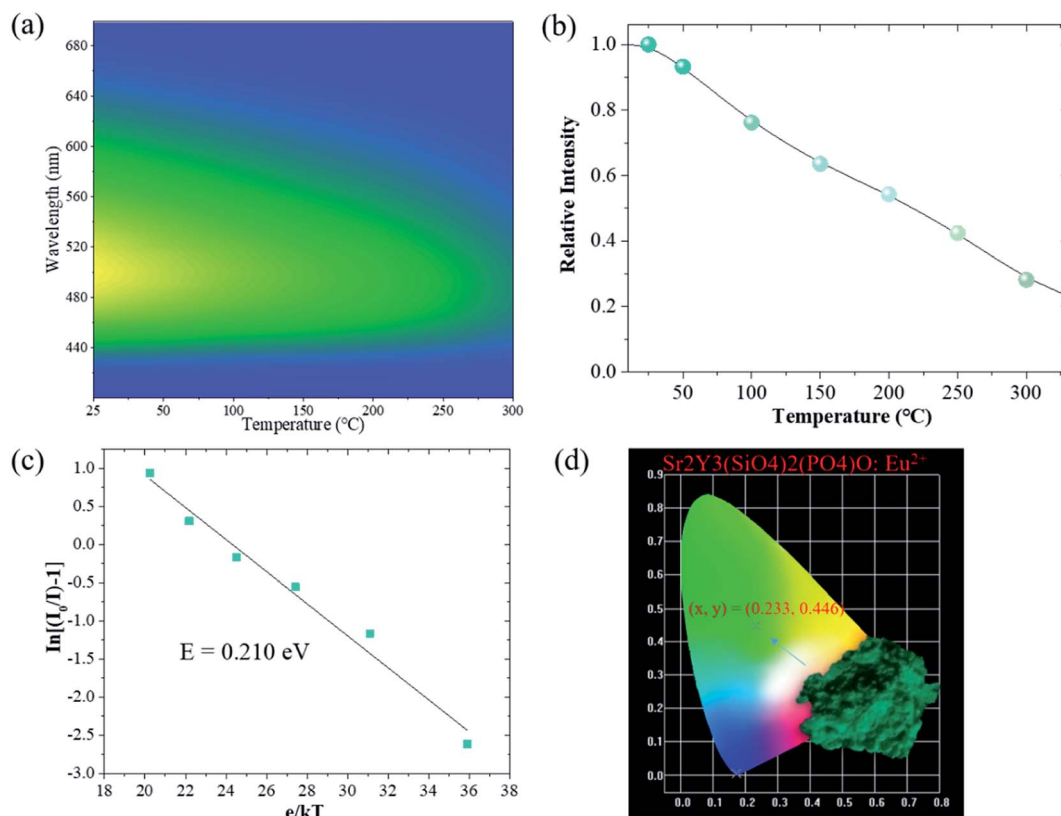
Fig. 6 (a) Temperature-dependent emission intensity of the $Sr_{3.95}Y_6(SiO_4)_4(PO_4)_2O_2$:0.05Eu^{2+} sample in the wavelength range of 400–700 nm, (b) temperature dependence of the emission intensity, (c) the plot of $\ln[(I_0/I_T) - 1]$ varied as a temperature function, (d) the CIE chromaticity coordinate diagram for $Sr_{3.95}Y_6(SiO_4)_4(PO_4)_2O_2$:0.05Eu^{2+} and the inset shows a digital photograph of the green-emitting phosphor.

emission can be observed clearly from the image of $Sr_{3.95}Y_6(SiO_4)_4(PO_4)_2O_2$:0.05Eu^{2+} at ultraviolet excitation.

4. Conclusions

A series of green phosphors $Sr_2Y_3(SiO_4)_2(PO_4)O_2$:Eu^{2+} with apatite structure were successfully synthesized *via* a traditional high-temperature solid-phase reaction and their luminescent properties were investigated. The phosphors generated a strong green emission band at 505 nm with an obvious broad band ranging from 400 to 700 nm. The determined optimal Eu^{2+} concentration of $Sr_2Y_3(SiO_4)_2(PO_4)O$:Eu^{2+} is 0.05. The experimental results and theoretical calculations suggest that the concentration quenching mechanism of Eu^{2+} in the $Sr_{3.95}Y_6(SiO_4)_4(PO_4)_2O_2$:0.05Eu^{2+} phosphor is d–d and the decay time of it was around 0.613 μs. All the investigations show that the as-prepared phosphor can be a green phosphor having potential research value.

Conflicts of interest

There are no conflicts to declare.

Acknowledgements

References

1 R. P. Cao, Y. L. Cao, T. Fu, S. H. Jiang, W. S. Li, Z. Y. Luo and J. W. Fu, Synthesis and luminescence properties of novel red-emitting $R_3P_4O_{13}$:Bi^{2+} (R = Sr and Ba) phosphors, *J. Alloys Compd.*, 2016, **661**, 77–81.

2 L. Li, X. H. Tang, Z. Q. Jiang, X. J. Zhou, S. Jiang, X. B. Luo, G. T. Xiang and K. N. Zhou, NaBaLa$_2$(PO$_4$)$_3$: A novel host lattice for Sm^{3+}-doped phosphor materials emitting reddish-orange light, *J. Alloys Compd.*, 2017, **701**, 515–523.

3 R. P. Cao, C. L. Liao, F. Xiao, G. T. Zheng, W. Hu, Y. M. Guo and Y. X. Ye, Emission enhancement of LiLaMo2O8:Eu^{3+} phosphor by co-doping with Bi3+ and Sm3+ ions, *Dyes Pigm.*, 2018, **149**, 574–580.

4 M. Runowski, S. Goderski, J. Paczesny, M. Księżopolska-Gocalska, A. Ekner-Grzyb, T. Grzyb, J. D. Rybka and M. Giersig, Stefan Lis Preparation of Biocompatible, Luminescent-Plasmonic Core/Shell Nanomaterials Based on Lanthanide and Gold Nanoparticles Exhibiting SERS Effects, *J. Phys. Chem. C*, 2016, **120**, 23788–23798.

5 W. Wang, H. Yang, Y. X. Liu, X. H. Yun, Y. Wei and G. G. Liu, (Ln^{3+} = Ce^{3+}, Eu^{3+})-doped oxyapatite-type phosphors, *CrystEngComm*, 2020, **22**, 311–319.

6 B. Han, Y. Z. Dai, J. Zhang, B. B. Liu and H. Z. Shi, Development of near-ultraviolet-excitable single-phase white-light-emitting phosphor $KBaY(BO_3)_2$:Ce^{3+},Dy^{3+} for phosphor-converted white light-emitting-diodes, *Ceram. Int.*, 2010, **71**, 1–34.

7 M. Runowski and S. Lis, Preparation and photophysical properties of luminescent nanoparticles based on lanthanide doped fluorides (LaF_3:Ce^{3+}, Gd^{3+}, Eu^{3+}), obtained in the presence of different surfactants, *J. Alloys Compd.*, 2014, **597**, 63–71.

8 P. Du, W. G. Ran, W. P. Li, L. H. Luo and X. Y. Huang, Morphology evolution of Eu^{3+}-activated $NaTbF_4$nanorods: a highly-efficient near-ultraviolet light-triggered red-emitting platform towards application in white light-emitting diodes, *RSC Adv.*, 2019, **7**, 10802–10809.

9 Q. Y. Bai, Z. J. Wang, P. L. Li, S. C. Xu, T. Li and Z. P. Yang, Zn_2–aGeO_4:aRE and Zn_2Ge1–aO_4:aRE (RE = Ce^{3+}, Eu^{3+}, Tb^{3+}, Dy^{3+}): 4f–4f and 5d–4f transition luminescence of rare earth ions under different substitution, *RSC Adv.*, 2016, **6**, 102183–102192.

10 W. J. Tang, Z. X. Huang and J. X. Liang, Controllable luminescence in Eu^{2+}-doped $Li_2Sr_4Al(PO_4)_3$ phosphor via tuning the Eu^{2+} concentration and codoping Ce^{3+}, *J. Alloys Compd.*, 2019, **778**, 612–617.

11 H. R. Li, Y. J. Liang, Y. L. Zhu, S. Q. Liu, J. H. Chen, H. Zhang and Y. J. Chen, Investigation of local structure distortion and electron cloud interaction on emission-band broadening induced by the concentration perturbation effect of cation substitution in $BaY_2Si_3O_{10}$:Eu phosphors, *CrystEngComm*, 2019, **21**, 4771–4785.

12 Q. Zhang, X. Ding and Y. H. Wang, Novel highly efficient blue-emitting $SrHfSi_2O_7$:Eu^{2+} phosphor: a potential color converter for WLEDs and FEDs, *Dyes Pigm.*, 2019, **163**, 168–175.

13 S. S. Lin, H. Lin, Q. M. Huang, Y. Cheng, J. Xu, J. M. Wang, X. Q. Xiang, C. Y. Wang, L. Q. Zhang and Y. S. Wang, Optical Storage: A Photostimulated $BaSi_2O_5$:Eu^{2+},Nd^{3+} Phosphor-in-Glass for Erasable-Rewritable Optical Storage Medium, *Laser Photonics Rev.*, 2019, **13**(4), 1863–8880.

14 M. Fei, Y. F. Tian, Z. Zhang, L. R. He, J. Chen, F. D. Bao, P. J. Zhang, Q. H. Zhang and L. Chen, The competitive mechanisms of nano-SiO_2 and reaction temperature on phase transformation and Eu^{2+} site occupation in Sr_2SiO_4:Eu^{2+} phosphor, *J. Alloys Compd.*, 2017, **728**, 231–240.

15 S. A. Khan, H. Zhong, W. W. Ji, N. Z. Khan, H. Abadikhah, L. Y. Hao, X. Xu, S. Agathopoulos and Q. L. Bao, Crystal-site engineering for developing tunable green light emitting $Ba_9Lu_2Si_6O_{24}$:Eu^{2+} phosphors for efficient white LEDs, *J. Alloys Compd.*, 2018, **767**, 374–381.

16 A. M. I. Ibrahim, Structural, electronic and optical properties of prominent $M_2Si_5N_8$:Eu^{2+} phosphors (M = Mg, Ca, Sr, Ba) from the ground–state and excited–state first principles calculations, *J. Alloys Compd.*, 2019, **775**, 30–38.

17 X. G. Zhang, F. W. Mo, Z. P. Zhu and Z. Y. Guo, Structure, site-occpancy and luminescent properties of a novel blue phosphor $Na_3ZrMgP_3O_{12}$:Eu^{2+}, *Mater. Res. Bull.*, 2018, **106**, 396–402.

18 P. Dorenbos, A Review on How Lanthanide Impurity Levels Change with Chemistry and Structure of Inorganic Compounds, *ECS J. Solid State Sci. Technol.*, 2013, **2**, R3001–R3011.

19 H. G. Guo, Y. H. Wang, G. Li, J. Y. Liu and Y. Y. Li, The persistent energy transfer of Eu^{2+} and Dy^{3+} and luminescence properties of a new cyan afterglow phosphor alpha-$Ca_3(PO_4)_2$:Eu^{2+}, Dy^{3+}, *RSC Adv.*, 2016, **6**, 101731–101736.

20 X. C. Wang, Z. Y. Zhao, Q. S. Wu, Y. Y. Li, C. Wang, A. J. Mao and Y. H. Wang, Synthesis, structure, and luminescence properties of $SrSiAl_2O_3N_2$:Eu^{2+} phosphors for light-emitting devices and field emission displays, *Dalton Trans.*, 2015, **44**, 11057–11066.

21 X. X. Ma, L. F. Mei, H. K. Liu, L. B. Liao, K. Nie, Y. Q. Liu and Z. H. Li, Synthesis and luminescence properties of Eu^{2+}-activated phosphor $Ba_3LaK(PO_4)3F$ for n-UV white-LEDs, *Polyhedron*, 2016, **119**, 223–226.

22 G. Li, Y. H. Wang, D. W. Liu, H. J. Guo and J. Liu, Cyan longlasting phosphorescence in green emitting phosphors $Ba_2Gd_2Si_4O_{13}$:Eu^{2+}, RE^{3+} (RE^{3+} = Dy^{3+}, Ho^{3+}, Tm^{3+}, Nd^{3+} and Tb^{3+}), *RSC Adv.*, 2016, **6**, 7024–7032.

23 S. M. Xu, K. Tang, T. Han, L. L. Luo and D. C. Zhu, Effect of Eu^{2+} on the luminescence properties of $Ba_{1.52-x}Zn_{0.2}Li_{0.4}SiO_4$:$0.05Ce^{3+}$, $0.03Mn^{2+}$, xEu^{2+} phosphor, *Optik*, 2016, **127**, 2370–2373.

24 B. Deng, J. Chen, H. Liu and C. S. Zhou, Photoluminescence properties of dysprosium doped novel apatite-type $Ba_2Y_3(SiO_4)_3$F white-emitting phosphor, *J. Mater. Sci.: Mater. Electron.*, 2019, **30**, 7507–7513.

25 N. Guo, C. Z. J. Jia, Y. F. Zhao, R. Z. Ouyang and W. Lu, White-Emitting Tuning and Energy Transfer in Eu^{2+}/Mn^{2+}-Substituted Apatite-Type Fluorophosphate Phosphors, *J. Am. Ceram. Soc.*, 2015, **98**, 1162–1168.

26 J. R. Peet, A. Piovano, M. R. Johnson and I. Radosavljevic Evans, Location and orientation of lone pairs in apatite-type materials: a computational study, *Dalton Trans.*, 2015, **98**(4), 1162–1168.

27 W. J. Tang and F. Zhang, A Single-Phase Emission-Tunable $Ca_5(PO_4)_3$F:Eu^{2+},Mn^{2+} Phosphor with Efficient Energy Transfer for White LEDs, *Eur. J. Inorg. Chem.*, 2014, **21**, 3387–3392.

28 S. J. Dhoble, Preparation and characterization of the $Sr_5(PO_4)_3$Cl:Eu^{2+} phosphor, *J. Phys. D: Appl. Phys.*, 2000, **33**(2), 158–161.

29 G. Seeta Rama Raju, J. Y. Park, G. P. Nagaraju, E. Pavitra, H. K. Yang, B. K. Moon, J. S. Yu, Y. S. Huh and J. H. Jeong, Evolution of $CaGd_2ZnO_5$:Eu^{3+} nanostructures for rapid visualization of latent fingerprints(Article), *J. Mater. Chem. C*, 2017, **5**, 4246–4256.

30 M. M. Shang, D. L. Geng, D. M. Yang, X. J. Kang, Y. Zhang and J. Lin, Luminescence and Energy Transfer Properties of $Ca_2Ba_3(PO_4)_3$Cl and $Ca_2Ba_3(PO_4)_3$Cl:A (A = Eu^{2+}/Ce^{3+}/
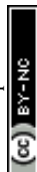
Dy^{3+}/Tb^{3+}) under UV and Low-Voltage Electron Beam Excitation, *Inorg. Chem.*, 2013, **52**, 3102–3112.

31 Bruker AXS, *TOPAS V4: General Profile and Structure Analysis Software for PowderDiffraction Data – User's Manual*, Bruker AXS, Karlsruhe, Germany, 2008.

32 Y. Z. Fang, F. X. Liu, J. S. Hou, Y. Zhang, X. F. Zheng, N. Zhang, G. Y. Zhao, M. S. Liao, G. Z. Dai, M. Q. Long and Y. F. Liu, Photoluminescence properties of blue light excited $Ca_8La_2(PO_4)_6O_2:Eu^{3+}$ red phosphors, *J. Lumin.*, 2016, **177**, 280–2885.

33 L. G. van Uitert, An empirical relation fitting the position in energy of the lower d-band edge for Eu^{2+} OR Ce^{3+} in various compounds, *J. Lumin.*, 1984, **29**, 1–9.

34 G. Blasse, Energy transfer in oxidic phosphors, *Phys. Lett. A*, 1968, **28**, 444–445.

35 J. Y. Sun, X. Y. Zhang, Z. G. Xia and H. Y. Du, Synthesis and luminescence properties of novel $LiSrPO_4:Dy^{3+}$, phosphor, *Mater. Res. Bull.*, 2011, **46**, 2179–2182.

36 L. M. Liang, L. F. Mei, H. K. Liu, C. C. Wang and L. B. Liao, Intense broad-band absorption and blue-emitting $Ca_9La(PO_4)_5(SiO_4)Cl_2:Eu^{2+}$ phosphor under near-ultraviolet excitation, *J. Lumin.*, 2019, **206**, 154–157.

37 Q. F. Guo, B. Ma, L. B. Liao, M. S. Molokeev, L. F. Mei and H. K. Liu, Crystal structure and luminescence properties of novel $Sr_{10-x}(SiO4)_3(SO_4)_3O:xEu^{2+}$ phosphor with apatite structure, *Ceram. Int.*, 2016, **42**, 11687–11691.

38 H. K. Liu, Y. Y. Zhang, L. B. Liao, Q. F. Guo and L. F. Mei, Synthesis, broad-band absorption and luminescence properties of blue-emitting phosphor $Sr_8La_2(PO_4)_6O_2:Eu^{2+}$ for n-UV white-light-emitting diodes, *Ceram. Int.*, 2014, **40**, 13709–13713.

39 B. Ramesha, G. Devarajulua, B. Deva Prasad Rajub, G. BhaskarKumarc, G. R. Dillipd, A. N. Banerjeed and S. W. Jood, Determination of strain, site occupancy,photoluminescent, and thermoluminescent-trapping parameters of Sm^{3+}-doped $NaSrB_5O_9$ microstructures, *Ceram. Int.*, 2016, **42**, 1234–1245.

40 H. Ye, M. Y. He, T. S. Zhou, Q. F. Guo, J. L. Zhang, L. B. Liao, L. F. Mei, H. K. Liu and M. Runowski, A novel reddish-orange fluorapatite phosphor, $La_{6-x}Ba_4(SiO_4)_6F_2:xSm^{3+}$ - Structure, luminescence and energy transfer properties, *J. Alloys Compd.*, 2018, **757**, 79–86.

41 S. Arrhenius, Über Die Reaktionsgeschwindigkeitbei der Inversion von RohrzuckerDurchSäuren, *Z. Phys. Chem.*, 1889, **4**, 226–248.

42 J. W. Qiao, L. X. Ning, M. S. Molokeev, Y. C. Chuang, Q. L. Liu and Z. Xia, Eu^{2+} site preferences in the mixed cation$K_2BaCa(PO_4)_2$ and thermally stable luminescence, *J. Am. Chem. Soc.*, 2018, **140**, 9730–9736.